Design and Validation of a Modular, Backdrivable Ankle Exoskeleton

Susan Zhao*, Katharine Walters*, José Montes Pérez, and Robert D. Gregg

***Abstract*— Partial-assist ankle exoskeletons have been limited by inherent trade-offs between favorable characteristics including high torque capacity, high control bandwidth, backdrivability, compliance, and low mass. Emerging quasi-direct drive actuators have a rigid transmission with a low gear ratio, enabling inherent backdrivability and compliance with accurate torque and position control. Our existing modular, backdrivable exoskeleton system (*M-BLUE*) uses quasi-direct drive actuators at the hip and/or knee to deliver high assistive torques alongside low dynamic backdrive torques, enabling natural interaction with users with remnant voluntary motion. This paper extends our modular system with the design and validation of a backdrivable ankle exoskeleton module to assist both plantarflexion and dorsiflexion. The bi-directional torque capabilities enable the study of control methods and gait outcomes for able-bodied users and users with gait impairments. Benchtop tests of the actuator performance and control bandwidth indicate that the position, voltage, and current control modes can provide assistance to the ankle joint across activities of daily living (ADLs). We also implement an optimal task-agnostic energy shaping controller for an experiment with a single human subject to validate the ability of the ankle exoskeleton to provide biomimetic torque assistance across a circuit of ADLs.**

I. Introduction

Partial assistance exoskeletons have the potential to assist users in their daily lives. In particular, the ankle joint performs significant positive work [1] and is responsible for a large portion of the total muscle energy expenditure [2] during gait. Ankle exoskeleton assistance has been shown to reduce effort for able-bodied individuals [3]–[9] and improve outcomes for individuals with gait impairments [10]–[13]. However, challenges remain in the design of ankle exoskeletons that can assist users across continuously varying activities of daily living (ADLs) outside the lab.

Some powered pneumatic [5], [14] and cable-driven [15], [16] devices off-board the actuators or power systems and use a tether to transmit force to an exoskeleton end-effector worn by the user, enabling both low mass and high torque capabilities. These tethered designs are suitable for studying control methods and gait outcomes across varying conditions in a lab or assisting gait rehabilitation in a clinical setting. However, tethered systems with large actuators requiring high power are not applicable for providing assistance outside the lab.

Passive ankle orthoses do not require external energy sources and can provide assistance outside the lab via mechanical energy storage or dissipation elements (e.g., spring or damper) that alter the impedance at the ankle joint. Impedance across the gait cycle can be controlled through passive elements that have customized stiffness and engagement [17], [18], cam profiles that enable variable stiffness as a function of ankle angle [12], [19], or clutch mechanisms that control the presence of stiffness during different gait phases [4], [8], [9]. The main benefit of passive devices is low mass compared to powered alternatives. However, fully passive devices can not provide net positive work for ADLs. Further, passive devices are optimized for a single task and can not actively adapt assistance to tasks requiring alternative stiffness profiles. Quasi-passive devices can adapt to varied gaits and slopes by actively controlling passive elements via a small, low-energy motor that varies stiffness or timing of assistance [20], [21] or via components that vary stiffness with electrical charge [22]. However, assistance provided by quasi-passive devices is inherently linked to the stiffness of the passive element [20]–[22] and adjusting assistance magnitudes for varying tasks or users would require replacing the passive element.

Untethered powered ankle exoskeletons use portable actuators worn by the user to perform positive work, and assistance can be actively controlled across varying tasks. Actuation systems with high transmission ratios (i.e., greater than 30:1) and a rigid connection from the motor to the joint enable accurate torque and position control [23], [24]. However, the lack of compliance and backdrivability restricts the user's movement to those enforced by the controller, limiting voluntary motion. Some designs with high transmission ratios achieved low backdrive torque during walking [25], [26], though inherently high mechanical impedance of the actuator restricts motions with high acceleration and makes open-loop torque control more difficult. Untethered pneumatic exoskeletons overcome these limitations with natural compliance and inherent backdrivability. However, these devices have limited peak torque [27], [28] and inherent trade-offs between slow response times for mobile compressors [28] or limited range for portable compressed gas sources [27].

Untethered cable-driven and powered-elastic actuation designs seek to enable high torque assistance while maintaining compliance and backdrivability. Cable-driven exoskeletons achieve high torque capabilities via a highly geared motor that applies a force about the ankle by spooling a belt or cord [3], [7], [10]. Applying force via a cable can enable the actuator to be placed at the hips [7], [10], reducing the metabolic burden of mass placed distally [29]. However, the highly geared motor must be controlled to reverse direction and allow cable slack to enable backdrivability. Series-elastic

This work was supported by the National Science Foundation Graduate Research Fellowship and by the National Institute of Biomedical Imaging and Bioengineering of the NIH under Award Number R01EB031166. The content is solely the responsibility of the authors.

S. Zhao, K. Walters, J. Montes Pérez, and R. D. Gregg are with the Department of Robotics, University of Michigan, Ann Arbor, MI 48109, USA. {susanmz, kwalte, jmontp, rdgregg}@umich.edu

*Indicates co-first authors.

actuation (SEA) enables inherent compliance by placing an elastic element between the motor and the load [11], [13], [30], which decouples the user from the motor inertia and can reduce electrical energy consumption in some cases [31]. However, SEA devices must be carefully characterized, and the output behavior (including backdrivability) may be a function of the individual component morphology, desired peak torque, and control strategy [16], [30]. A magnetorheological clutch placed between a highly geared motor and the ankle overcame this limitation by decoupling the motor inertia from the ankle, enabling high velocity and high bandwidth performance while maintaining backdrivability [6]. However, the high performance comes at the cost of high mass (6.2 kg for the bilateral system).

Quasi-direct drive actuation has a rigid transmission with a low gear ratio, enabling inherent backdrivability and compliance with accurate torque and position control [32], [33] while overcoming traditional limitations of rigid transmissions [34]. Our existing Modular Backdrivable Lower-limb Unloading Exoskeleton (M-BLUE) system uses quasi-direct drive actuators to provide partial assistive torque to the knee and hip [35]. The low static and dynamic backdrive torque promotes natural interaction with users with remnant voluntary motion, and torque assistance for hip/knee configurations was shown to decrease muscle effort for various activities [36]. We previously implemented a task-agnostic energy shaping controller on a belt-driven, low-ratio ankle exoskeleton [37]. However, torque assistance was inherently limited to plantarflexion and the nonlinear belt-driven transmission required discrete switching between current control during stance and position control during swing.

In this paper, we extend our modular, partial assistance exoskeleton system with the design and validation of a backdrivable ankle exoskeleton module capable of assisting both plantar- and dorsi-flexion. To the author's knowledge, this is the first quasi-direct drive ankle exoskeleton. The bi-directional assistance capabilities enable the study of control methods and gait outcomes for able-bodied users and users with gait impairments (e.g., due to cerebral palsy [10] or following a stroke [17]). We show the ankle module integration with the existing knee and hip modules of M-BLUE and characterize the motor control bandwidth of the position, current, and voltage control modes. We further validate the performance of the exoskeleton by extending an optimal task-agnostic energy shaping controller for plantar-flexion assistance [37] to assist both plantar- and dorsi-flexion and implementing the controller with a single subject case study over multiple ADLs requiring high control bandwidth.

II. Mechanical Design and Characterization

In this section, we detail the mechanical design of the ankle exoskeleton module, its integration with the existing hip and/or knee M-BLUE configurations, and benchtop tests to characterize actuator performance.

A. Design

The modular ankle exoskeleton design is portable, lightweight, and capable of assisting both plantar- and dorsi-flexion. We extend the existing M-BLUE actuation paradigm of providing partial assistive torque with low backdrive torque by selecting the same highly backdrivable, compact and torque-dense actuator for the ankle module. The T-motor AK80-9 with the Dephy FASTER motor driver is a quasi-direct drive actuator with a 9:1 planetary gearset, providing up to 30Nm peak torque with less than 2Nm of dynamic backdrive torque during human-like walking motions [35]. The actuator's low-level control is executed by the Dephy FASTER motor driver system (Dephy Inc., Maynard, MA), which includes built-in functionality for position, voltage (velocity), and current (torque) control. We ran our high-level controller on a Raspberry Pi 4B with 8GB RAM which communicates with the actuator via USB. The system is powered by a 24V, 2.0Ah lithium-ion battery (Kobalt).

For the exoskeleton structural design, we fabricated two custom parts from 1/8" aluminum sheet-metal (7075-T6) to mount the actuator and interface with the user (Fig. 1). The lower ankle component is fastened to the shaft of the actuator via six bolts and is secured to a carbon fiber plate in the sole of a boot with two threaded fasteners. The motor output is aligned approximately co-axial with the sagittal degree-of-freedom of the ankle joint. We selected the commercial Dephy boot typically interfaced with the Exoboot ankle exoskeleton (Dephy Inc., Maynard, MA), though future alternatives could include custom fabricated options. The upper ankle component fastens to the housing of the actuator via eight bolts and enables the shank of the exoskeleton to be secured to the user with a strap. The aluminum structural components in combination with the carbon fiber plate in the sole of the boot act as the torque transfer linkage, allowing the actuator to apply assistive torque in both directions. The mass of the structural components (i.e., aluminum uprights) and motor is 655g. The shank cuff adds 95g, and a men's size 10US boot adds 430g. The sensors required for energy shaping control (Sec. III) add 470g unilaterally, and the micro-controller and battery (worn on the torso) add 635g. A bilateral system can be powered and controlled via a single micro-computer and battery. The total unilateral system weighs 2.3kg.

The shank of the ankle exoskeleton is secured to the user via a pad and strap from a commercially available orthosis, similar to the original M-BLUE design [35]. The ankle-only module uses the lower lateral pad and strap on a telescoping sleeve with a lock clip from the T Scope Premier Post-Op Knee Brace (Breg, California, USA), which is the same orthosis used in the original knee module. The telescoping sleeve is freely adjustable along the height of the upper ankle structural component to accommodate a wide range of user heights. The lock clip prevents translation of the shank strap following adjustment to the desired height. The pad and strap can be positioned and tightened at the calf to the user's compliance and comfort. The two threaded screws at the boot

Fig. 1. **M-BLUE ankle exoskeleton module and components.**

provides a simple interface with a quick and easy process to change out boots for sizing.

B. Modular Configurations

Previous work has shown that the M-BLUE knee and hip modules can operate independently or in conjunction [35]. The addition of the ankle module enables hip-ankle, knee-ankle, and hip-knee-ankle configurations (Fig. 2). The hip-ankle configuration consists of the standalone hip and ankle modules with no physical connection between the modules. For the knee-ankle and hip-knee-ankle configurations, the knee and ankle modules must be connected. We did this by removing the telescoping shank pad and strap from the ankle and knee modules, drilling four holes in the lower knee aluminum upright, attaching a fixed pad to the knee module, and using two screws with cam handles to secure the ankle to the knee (Fig. 2). The upper ankle component is fastened to the knee module through a slot, enabling adjustability to accommodate users of varying heights.

Fig. 2. **M-BLUE configurations with the ankle module.** The knee-ankle, hip-ankle, and hip-knee-ankle configurations are shown from left to right. The rightmost diagram illustrates the attachment of ankle and knee modules.

The extension of the M-BLUE system to three modular powered joints enables adaptability and freedom to explore single-joint, multi-joint, or whole-leg assistance. Many factors must be considered when determining the optimal configuration based on user needs and priorities. Assistance using a hip-knee-ankle exoskeleton has been found to reduce the metabolic cost of walking more than assistance at one or two joints [38]. However, a targeted single or double joint configuration may prove more advantageous if considering factors such as activity, weight, bulk, cost and overall system complexity. This paper focuses on characterizing and validating the new ankle module alone, leaving investigation and validation of multi-joint configurations to future work.

C. Actuator Characterization

The AK80-9 actuator was previously characterized to produce a peak torque of 30Nm with dynamic backdrive torque of 2Nm, though the step response performance was not reported [35]. Another previous study characterized the performance and thermal properties of the T-motor U8-KV100, an electric motor nearly identical to the one inside the AK80-9 [39]. However, the transmission dynamics of the 9:1 planetary gearset integrated with the electric motor in the AK80-9 influence the open-loop control performance and has not yet been characterized. In this paper, we extend the characterization of the AK80-9 to account for the transmission dynamics in the open-loop step response.

The actuator performance and open-loop control bandwidth of the position, voltage, and current control modes was characterized by a set of step-input and frequency response tests. For the position and voltage control tests, the actuator was mounted with the shaft able to freely spin, and a magnetic rotary joint encoder (AK02 Encoder, Dephy) recorded the output shaft position and velocity. For the current control tests, a single-axis 100Nm capacity rotary torque sensor (TRS605, FUTEK, Irvine, CA, USA) was secured within the common rotational shaft to measure the actuator output torque (Fig. 3). A 50:1 gearbox was coupled to the rotational shaft on the output of the torque sensor and the shaft was mechanically grounded.

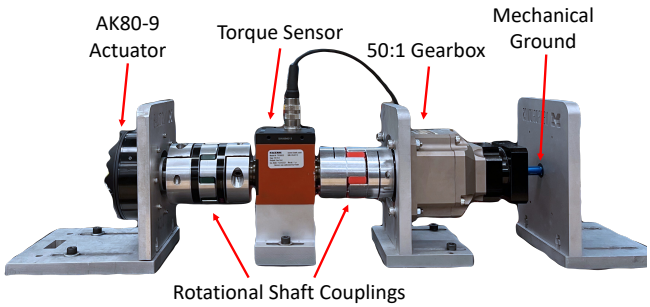

Fig. 3. **Open-loop current control testing benchtop setup.**

Current control tests characterize the open-loop torque control performance, where the open-loop torque is a function of control current according to $\tau_{\text{output}} = i^q \cdot K_t \cdot N$, where i^q is the q-axis current (A), K_t is the torque constant (Nm/A), and $N = 9$ is the gear ratio. Output torque is defined as the torque (Nm) on the output shaft of the actuator that would be applied to the joint. As we are using a newer model of the actuator than the one used for the hip and/or knee modules, the torque constant is slightly different than

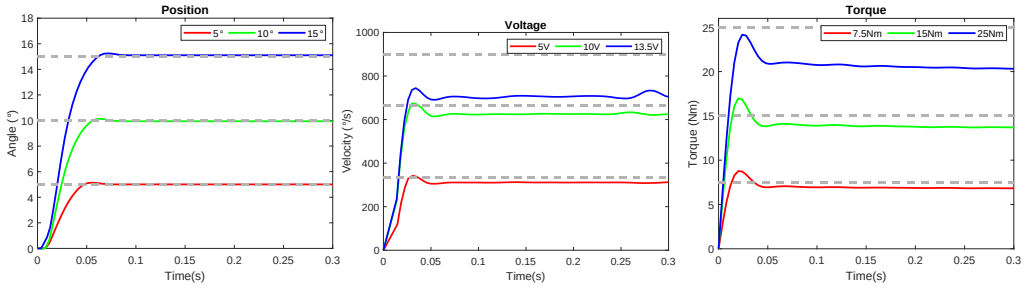

Fig. 4. **Average step response results** for each input magnitude for position (a), voltage (b), and torque (i.e., current) (c) control modes. Dashed lines are the reference values.

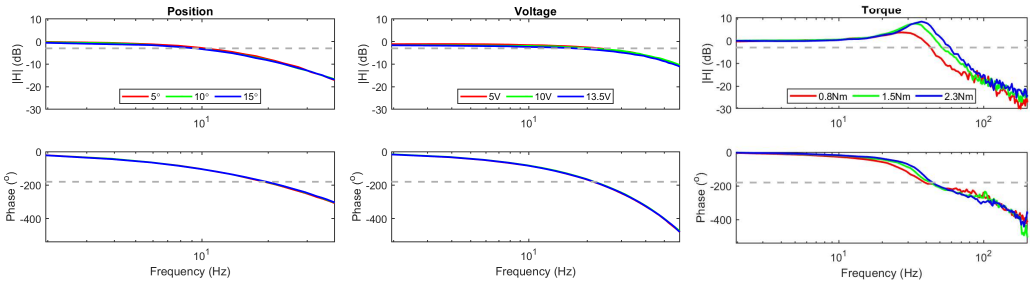

Fig. 5. **Average frequency response results** for each input magnitude for position (a), voltage (b), and current (c) control modes. Dashed lines represent -3dB and -180° phase. Bandwidth was determined by where the frequency magnitude crossed -3dB.

the one previously reported [35]. We empirically calculated the torque constant by driving the unpowered actuator at a constant velocity with an electric drill and finding the back-emf constant for two motor phases. The q-axis back-emf constant is given by $K_b^q = \overline{V}^{ll} / \left(\sqrt{\frac{2}{3}} \frac{d\theta_m}{dt} \right)$, where $\overline{V}^{ll}$ is the line-to-line voltage and $\frac{d\theta_m}{dt}$ is the magnetic angular velocity. The torque constant for our actuator, $K_t = 0.112$ Nm/A, is equivalent to the q-axis back-emf constant.

Step response tests quantified the performance of the open-loop control modes in the time domain. For position control (Fig. 4a), reference step inputs were commanded at 5°, 10°, and 15°. The low-level proportional position controller was hand-tuned with gain $k_p = 50$. For voltage control (Fig. 4b), reference step inputs were commanded at 5V, 10V, and 13.5V which correspond to output angular velocities of 333°/s, 666°/s, and 900°/s respectively. The open-loop output velocity (°/s) is a function of the control voltage according to $\omega_{\text{output}} = V \cdot \frac{1}{k_v} \cdot \frac{1}{N}$, where V (volts) is the control voltage, $k_v = 0.00167$ (V/°/s) is the motor voltage constant, and $N = 9$ is the gear ratio. The voltage conditions were selected to characterize the control performance at ankle angular velocities for human walking (250°/s) and vertical jumping (900°/s) [6]. For current control (Fig. 4c), reference step inputs were commanded at 7.4A, 14.9A, and 24.8A, which correspond to output torque values of 7.5Nm, 15Nm, and 25Nm respectively. The 7.5Nm torque input corresponds to the peak average dorsiflexion torque for a 100kg human walking at 1.5m/s, and the 25Nm torque input corresponds to the maximum step input for the previous actuator characterization [35]. The low-level current controller used proportional $k_p = 40$, integral $k_i = 400$, and feed-forward $k_{ff} = 128$ gains recommended by Dephy. For each condition we collected five trials, each having a duration of 3 seconds with the exception of the 25Nm step input which had a duration of 1 second to respect the actuator thermal limits. We calculated the rise time, settling time, overshoot and steady-state error for each trial and averaged the results for each condition. To reduce noise in the calculation of the step response performance, we filtered the output velocity and current using a third order Butterworth filter with a cutoff frequency of 100Hz and a zero-phase digital filter.

Frequency tests characterized the open-loop control bandwidth of the position, voltage, and current control modes in the frequency domain (Fig. 5). The reference input trajectories were Gaussian white noise signals, low-pass filtered using a third order Butterworth filter. The cutoff frequency for the position trajectories was 40Hz, and the signal was scaled to magnitudes of $\pm 5°$, $\pm 10°$, and $\pm 15°$. The cutoff frequency for the voltage trajectories was 60Hz, and the signal was scaled to magnitudes of 5V, 10V, and 13.5V. The cutoff frequency for the current trajectories was 200Hz, and the signal was scaled to magnitudes of 0.8A, 1.5A, and 2.3A, corresponding to torque magnitudes of 0.8Nm, 1.5Nm, and 2.3Nm, respectively. Data for each condition were sampled at a rate of 1000Hz. Five trials were collected for each condition, each with a duration of 30 seconds. The frequency response was determined through Bode plots using Welch's averaged periodogram method. We calculated the control bandwidth for each trial as the frequency where the frequency response magnitude crossed -3dB and averaged the trials for each condition.

D. Actuator Performance and Control Bandwidth Results

The open-loop control performance and bandwidth averaged across all conditions for position, voltage, and current

control modes are given in Table I. The step response performance is characterized by the rise time in milliseconds, settling time in milliseconds, overshoot as a percentage of the steady-state response, and steady-state error as a percentage of the desired response. The range of control bandwidths is reported for each control mode.

TABLE I

ACTUATOR CHARACTERIZATION RESULTS

	Position	**Voltage**	**Current**
Rise Time (ms)	30.9 ± 3.8	18.5 ± 1.1	10.1 ± 1.4
Settling Time (ms)	57.8 ± 4.8	77.2 ± 56.8	85.3 ± 32.2
Overshoot (%)	1.8 ± 0.8	6.8 ± 2.5	23.2 ± 4.5
Steady-state Error (%)	0.8 ± 0.4	10.7 ± 7.7	13.4 ± 6.6
Bandwidth (Hz)	9 ∼ 11	17 ∼ 23	42 ∼ 60

III. CONTROLLER IMPLEMENTATION AND VALIDATION

In this section, we implement an energy shaping controller for assisting plantar- and dorsi-flexion, extending a controller previously designed for plantarflexion only [37]. A single subject traversing a circuit of ADLs involving both high velocities and high torques demonstrates the performance of our ankle exoskeleton design.

A. Optimal Energy Shaping Controller

Energy shaping control does not enforce kinematic trajectories and enables task-agnostic assistance by calculating control torque as a function of the instantaneous system angles. We briefly review the system model presented in detail in [37]. Two links representing the shank and foot are joined by a revolute joint representing the ankle (Fig. 6). The global foot angle ϕ is defined relative to the vertical, and θ is the relative ankle angle.

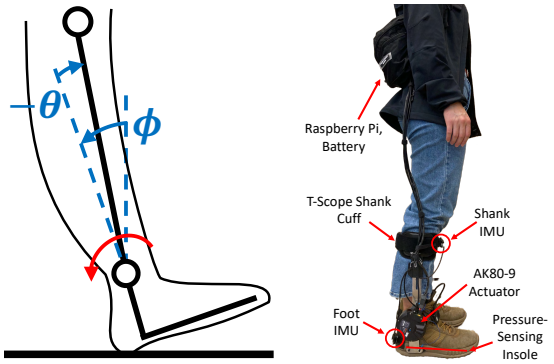

Fig. 6. **System model and hardware setup**.

To design a controller to apply biomimetic torque across varying tasks and users, we formulate a convex optimization over a basis function representation of the space of possible controllers. The trigonometric basis functions previously used to provide task-agnostic torque assistance during stance are defined by the set,

$$\zeta(q) = \{1, \psi, \sin(\psi), \cos(\psi), \sin(2\psi), \cos(2\psi), \phi, \sin(\phi), \cos(\phi), \sin(2\phi), \cos(2\phi)\},$$

where $\psi = \phi - \theta$ is the global shank angle [37]. We define $\alpha \in \mathbb{R}^{11\times 1}$ and $\delta \in \mathbb{R}^{11\times 1}$ as vectors of scalar coefficients.

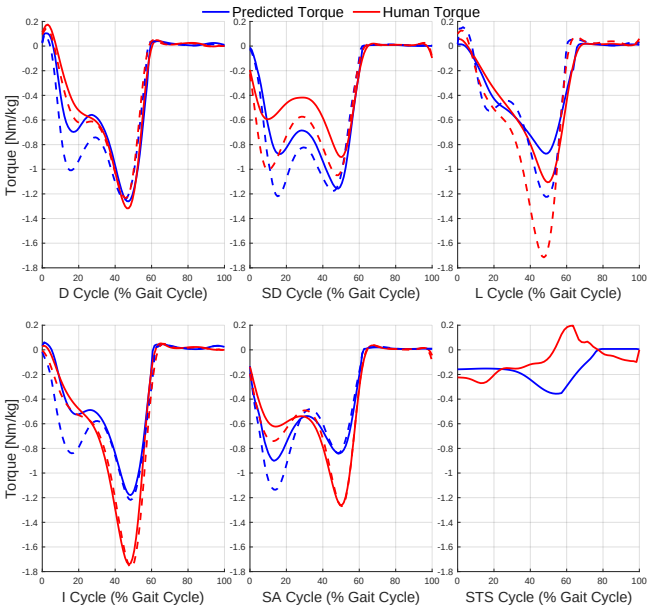

Fig. 7. **Simulated controller torque** across steady-state ADLs for inter-subject average kinematic inputs from the training dataset. The controller was optimized across ramp decline (D) at 5.2° (solid) and 11° (dashed), stair descent (SD) at 4in (solid) and 7in (dashed) step heights, level walking (L) at 0.5m/s (solid) and 1.5m/s (dashed), ramp incline (I) at 5.2° (solid) and 11° (dashed), stair ascent (SA) at 4in (solid) and 7in (dashed) step heights, and stand-to-sit (STS).

We define the control law,

$$u = \beta(vGRF) \cdot vGRF \cdot \zeta(q) \cdot \alpha + (1 - \beta(vGRF)) \cdot \zeta(q) \cdot \delta, \quad (1)$$

where $vGRF$ is the vertical ground reaction force normalized by mass between 0 (swing) and 1 (single-support stance). The coefficients α were previously used to apply plantarflexion assistance [37] and the coefficients δ scale the basis functions ζ to apply dorsiflexion assistance. The sigmoid function $\beta(vGRF) = 1/(1+e^{-50(vGRF-0.1)})$ tapers the torque between stance and swing such that $\beta(vGRF) = 1$ during stance and $\beta(vGRF) = 0$ during swing. As the sigmoid function of the $vGRF$ smoothly switches the calculation of control torque between two vectors of coefficients, the coefficients α and δ separately approximate biomimetic torque for stance and swing phases, respectively. We optimize the coefficients α and δ to minimize the error between control torque and human torque over a range of tasks and subjects from a published able-bodied dataset [37]. As normative dorsiflexion torque magnitudes are small compared to plantarflexion, we apply a higher weight on the error between control torque and normative torque for swing phase across all tasks.

The simulated controller performance for inter-subject average steady-state kinematic inputs from the training dataset is shown in Fig. 7. The performance during stance is similar to [37], and during swing the controller reasonably approximates dorsiflexion torque across all ambulatory tasks. The simulated controller briefly applies torque of the opposite sign for stand-to-sit. However, the torque magnitude is low compared to other tasks and it was previously noted that users could not perceive the discrepancy in torque sign [37].

Further, the normative human torque comparison for stand-to-sit is only for a single subject and it is possible that this single subject is not representative of the population.

B. Human Subject Experiment

To implement the novel energy shaping controller, inertial measurement units (IMUs) are mounted on the shank and foot to provide the global link angles (3DM-GX5-25, Lord MicroStrain). The difference between these two signals gives a better estimate of ankle angle than the motor encoder due to compliance in the mechanical interface. A pressure-sensing insole is placed under the user's foot in the boot to approximate the vGRF (Actisense, IEE, Luxembourg). The control torque is multiplied by the user's mass and specified level of assistance (%LOA).

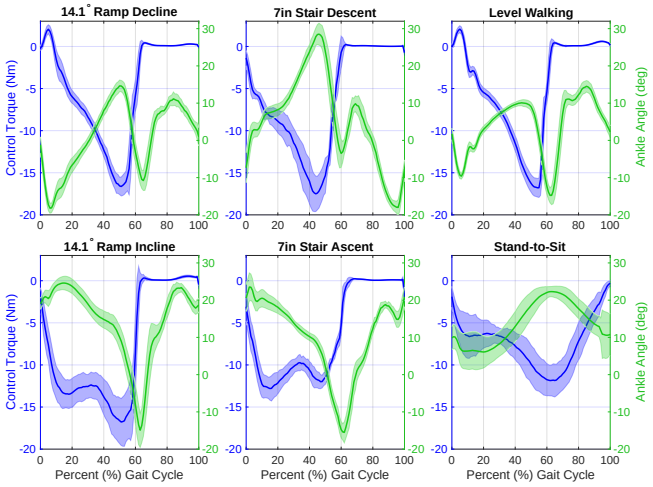

Fig. 8. **Energy shaping control performance** for the average stride on each circuit task. Solid lines indicate the mean and shaded regions indicate ± 1 standard deviation.

To validate the performance of the ankle exoskeleton across ADLs, n=1 (female, 1.63m, 64kg) human subject performed varying ambulatory tasks on a circuit at a self-selected speed while wearing a unilateral ankle exoskeleton. The participant acclimated to the ankle exoskeleton assistance by practicing across the circuit while incrementally increasing the %LOA to find the preferred %LOA (or motor saturation is reached). The exoskeleton is capable of providing up to roughly 25% normative ankle torque (depending on task and user mass). During the experiment, the participant traversed the circuit ten times in the clockwise (CW) direction and ten times in the counterclockwise (CCW) direction. The CW direction consisted of sit-to-stand, 14.1° ramp incline, 7in stair descent, level walking, and stand-to-sit. The CCW direction consisted of sit-to-stand, level walking, 7in stair ascent, 14.1° ramp descent, and stand-to-sit. The study was approved by the University of Michigan IRB under protocol HUM00201957. Strides were parsed at heelstrikes using the vGRF calculated by the pressure-sensing insole and task for each stride was determined with a video recording of the trial.

The control torque and ankle angle for the single human subject's average circuit strides are shown in Fig. 8. The strides are defined as those occurring heelstrike to heelstrike on the task and the control torque is defined as the body-mass normalized control torque calculated by (1). The controller provides roughly biomimetic plantarflexion and dorsiflexion torque across the range of tasks.

IV. Discussion

We presented the design and validation of a modular, backdrivable partial assistance ankle exoskeleton. The quasi-direct drive actuator with 9:1 gear ratio enables inherent compliance and backdrivability. The simple two-part structural design and the use of commercially available orthosis components and boots to interface with the user enables simple system preparation for control method and gait outcome research. Further, the custom aluminum structural components aligning the actuator co-axial with the ankle joint and the integration of the Dephy FASTER motor driver enable simple position, voltage (velocity), and current control. The total unilateral system mass is 2.3 kg and the peak torque is 30Nm, which is comparable to torque-to-weight ratios of existing designs [7], [37].

Actuator benchtop testing characterized the open-loop step input tracking and control bandwidth for position, voltage, and current control modes. The integrated motor driver achieves fast rise and settling times for step inputs while maintaining low overshoot. The rigid transmission enables accurate position control, but the dynamics in the transmission result in increasing steady-state error with increasing voltage and current step magnitude. Further, the dynamics of the 9:1 transmission reduced the position and current control bandwidths reported for a similar electric motor with no transmission [39]. However, our actuator control bandwidths for position (9-11 Hz), voltage (17-23 Hz), and current control (42-60 Hz) are more than sufficient to assist the ankle joint across ADLs.

We extended a previous task-agnostic optimal energy shaping controller for plantarflexion to provide biomimetic torque assistance across both stance and swing. A small set of trigonometric basis functions of the global shank and foot angles scaled by optimized scalar coefficients can capture relationships between kinematics and plantarflexion and dorsiflexion torque peaks across tasks, enabling continuous assistance across the gait cycle without discrete mode switching at heelstrike and toe-off. The energy shaping control implementation and performance validation demonstrates comparable plantarflexion assistance across varying ADLs to previous work [37]. The addition of task-agnostic dorsiflexion assistance expands the ability of this exoskeleton to benefit populations requiring bi-directional torque assistance.

Our design has some limitations. By empirically calculating the torque constant for a single velocity, we did not account for friction in the transmission that nonlinearly affects the torque-current relationship [35]. The open-loop torque command has resulting steady-state error for step inputs. We will seek to improve the actuator torque model and reduce the steady-state error in future work. However, the simple empirical estimate of the torque constant in combination with

the integrated Dephy low-level controller achieved output torques within roughly 13% of the desired step input torque. The simple out-of-the-box low-level control enables research for high-level control methods and gait outcomes.

ACKNOWLEDGEMENT

The authors thank Christopher Nesler, Gray C. Thomas, Yichen Wang, and Riley Pieper for their assistance.

REFERENCES

[1] M. Meinders, A. Gitter, and J. M. Czerniecki, "The role of ankle plantar flexor muscle work during walking." *Scand J Rehab Med*, vol. 30, no. 1, pp. 39–46, 1998.

[2] B. R. Umberger and J. Rubenson, "Understanding muscle energetics in locomotion: new modeling and experimental approaches," *Exerc Sport Sci Rev*, vol. 39, no. 2, pp. 59–67, 2011.

[3] L. M. Mooney, E. J. Rouse, and H. M. Herr, "Autonomous exoskeleton reduces metabolic cost of human walking during load carriage," *J NeuroEngineering Rehabil*, vol. 11, no. 1, pp. 1–11, 2014.

[4] S. H. Collins, M. B. Wiggin, and G. S. Sawicki, "Reducing the energy cost of human walking using an unpowered exoskeleton," *Nature*, vol. 522, no. 7555, pp. 212–215, 2015.

[5] D. P. Ferris, J. M. Czerniecki, and B. Hannaford, "An ankle-foot orthosis powered by artificial pneumatic muscles," *J. Applied Biomechanics*, vol. 21, no. 2, pp. 189–197, 2005.

[6] C. Khazoom, C. Véronneau, J.-P. L. Bigué, J. Grenier, A. Girard, and J.-S. Plante, "Design and control of a multifunctional ankle exoskeleton powered by magnetorheological actuators to assist walking, jumping, and landing," *IEEE Robot Autom Lett*, vol. 4, no. 3, pp. 3083–3090, 2019.

[7] Y. Bougrinat, S. Achiche, and M. Raison, "Design and development of a lightweight ankle exoskeleton for human walking augmentation," *Mechatronics*, vol. 64, p. 102297, 2019.

[8] M. B. Yandell, J. R. Tacca, and K. E. Zelik, "Design of a low profile, unpowered ankle exoskeleton that fits under clothes: overcoming practical barriers to widespread societal adoption," *IEEE Trans Neural Syst Rehabil Eng*, vol. 27, no. 4, pp. 712–723, 2019.

[9] S. Pardoel and M. Doumit, "Development and testing of a passive ankle exoskeleton," *Biocybern. Biomed. Eng.*, vol. 39, no. 3, pp. 902–913, 2019.

[10] Z. F. Lerner, G. M. Gasparri, M. O. Bair, J. L. Lawson, J. Luque, T. A. Harvey, and A. T. Lerner, "An untethered ankle exoskeleton improves walking economy in a pilot study of individuals with cerebral palsy," *IEEE Trans Neural Syst Rehabil Eng*, vol. 26, no. 10, pp. 1985–1993, 2018.

[11] J. A. Blaya and H. Herr, "Adaptive control of a variable-impedance ankle-foot orthosis to assist drop-foot gait," *IEEE Trans Neural Syst Rehabil Eng*, vol. 12, no. 1, pp. 24–31, 2004.

[12] Y. Sekiguchi, D. Owaki, K. Honda, K. Fukushi, N. Hiroi, T. Nozaki, and S.-i. Izumi, "Ankle–foot orthosis with dorsiflexion resistance using spring-cam mechanism increases knee flexion in the swing phase during walking in stroke patients with hemiplegia," *Gait & Posture*, vol. 81, pp. 27–32, 2020.

[13] J. Ward, T. Sugar, A. Boehler, J. Standeven, and J. R. Engsberg, "Stroke survivors' gait adaptations to a powered ankle–foot orthosis," *Advanced Robotics*, vol. 25, no. 15, pp. 1879–1901, 2011.

[14] Y.-L. Park, B.-r. Chen, D. Young, L. Stirling, R. J. Wood, E. Goldfield, and R. Nagpal, "Bio-inspired active soft orthotic device for ankle foot pathologies," in *IEEE/RSJ Int. Conf. Intell. Robots Syst.*, vol. 8, 2011, pp. 25–30.

[15] J. Bae *et al.*, "A soft exosuit for patients with stroke: Feasibility study with a mobile off-board actuation unit," in *2015 IEEE Int. Conf. Rehabilitation Robotics (ICORR)*, 2015, pp. 131–138.

[16] K. A. Witte, J. Zhang, R. W. Jackson, and S. H. Collins, "Design of two lightweight, high-bandwidth torque-controlled ankle exoskeletons," in *2015 IEEE Int. Conf. Robot Autom.*, 2015, pp. 1223–1228.

[17] T. Kobayashi, M. S. Orendurff, G. Hunt, L. S. Lincoln, F. Gao, N. LeCursi, and K. B. Foreman, "An articulated ankle–foot orthosis with adjustable plantarflexion resistance, dorsiflexion resistance and alignment: A pilot study on mechanical properties and effects on stroke hemiparetic gait," *Med. Eng. Phys.*, vol. 44, pp. 94–101, 2017.

[18] S. Yamamoto, A. Hagiwara, T. Mizobe, O. Yokoyama, and T. Yasui, "Development of an ankle–foot orthosis with an oil damper," *Prosthetics and orthotics international*, vol. 29, no. 3, pp. 209–219, 2005.

[19] K. Rodriguez, J. De Groot, F. Baas, M. Stijntjes, F. Van Der Helm, H. Van Der Kooijl, and W. Mugge, "Passive ankle joint stiffness compensation by a novel ankle-foot-orthosis," in *2018 7th IEEE RAS EMBS Int. Conf. Biomed. Robot. Biomechatron.*, 2018, pp. 517–522.

[20] C. Wang *et al.*, "Design of an ankle exoskeleton that recycles energy to assist propulsion during human walking," *IEEE Trans. Biomedical Engineering*, vol. 69, no. 3, pp. 1212–1224, 2021.

[21] A. Polinkovsky, R. J. Bachmann, N. I. Kern, and R. D. Quinn, "An ankle foot orthosis with insertion point eccentricity control," in *2012 IEEE/RSJ Int. Conf. Intell. Robots Syst.*, 2012, pp. 1603–1608.

[22] D. P. Allen, R. Little, J. Laube, J. Warren, W. Voit, and R. D. Gregg, "Towards an ankle-foot orthosis powered by a dielectric elastomer actuator," *Mechatronics*, vol. 76, p. 102551, 2021.

[23] Y. Bai, X. Gao, J. Zhao, F. Jin, F. Dai, and Y. Lv, "A portable ankle-foot rehabilitation orthosis powered by electric motor," *Open Mech. Eng. J.*, vol. 9, no. 1, 2015.

[24] D. Gomez-Vargas, F. Ballen-Moreno, P. Barria, R. Aguilar, J. M. Azorín, M. Munera, and C. A. Cifuentes, "The actuation system of the ankle exoskeleton t-flex: First use experimental validation in people with stroke," *Brain sciences*, vol. 11, no. 4, p. 412, 2021.

[25] M. Lee *et al.*, "A compact ankle exoskeleton with a multiaxis parallel linkage mechanism," *IEEE/ASME Trans. Mechatron.*, vol. 26, no. 1, pp. 191–202, 2020.

[26] G. Lv, H. Zhu, T. Elery, L. Li, and R. D. Gregg, "Experimental implementation of underactuated potential energy shaping on a powered ankle-foot orthosis," in *IEEE Int. Conf. Robot Autom.*, 2016, pp. 3493–3500.

[27] K. A. Shorter, G. F. Kogler, E. Loth, W. K. Durfee, and E. T. Hsiao-Wecksler, "A portable powered ankle-foot orthosis for rehabilitation," *J. Rehabil. Res. Dev*, vol. 48, no. 4, pp. 459–472, 2011.

[28] S. J. Kim, Y. Na, D. Y. Lee, H. Chang, and J. Kim, "Pneumatic afo powered by a miniature custom compressor for drop foot correction," *IEEE Trans. Neural Syst. Rehabil. Eng*, vol. 28, no. 8, pp. 1781–1789, 2020.

[29] R. C. Browning, J. R. Modica, R. Kram, and A. Goswami, "The effects of adding mass to the legs on the energetics and biomechanics of walking," *Med. Sci. Sports Exerc.*, vol. 39, no. 3, pp. 515–525, 2007.

[30] Y. Shao, W. Zhang, Y. Su, and X. Ding, "Design and optimisation of load-adaptive actuator with variable stiffness for compact ankle exoskeleton," *Mech. Mach. Theory*, vol. 161, p. 104323, 2021.

[31] E. A. B. Nieto, S. Rezazadeh, and R. D. Gregg, "Minimizing energy consumption and peak power of series elastic actuators: A convex optimization framework for elastic element design," *IEEE/ASME Trans. Mechatronics*, vol. 24, no. 3, pp. 1334–1345, 2019.

[32] H. Zhu, C. Nesler, N. Divekar, V. Peddinti, and R. D. Gregg, "Design principles for compact, backdrivable actuation in partial-assist powered knee orthoses," *IEEE/ASME Trans. Mechatron.*, vol. 26, no. 6, pp. 3104–3115, 2021.

[33] B. Laschowski and J. McPhee, "Energy-efficient actuator design principles for robotic leg prostheses and exoskeletons: A review of series elasticity and backdrivability," *J. Comput. Nonlin. Dyn.*, vol. 18, no. 6, p. 060801, 2023.

[34] J. S. Lora-Millan, M. Nabipour, E. van Asseldonk, and C. Bayón, "Advances on mechanical designs for assistive ankle-foot orthoses," *Front. Bioeng. Biotechnol.*, vol. 11, 2023.

[35] C. Nesler, G. Thomas, N. Divekar, E. J. Rouse, and R. D. Gregg, "Enhancing voluntary motion with modular, backdrivable, powered hip and knee orthoses," *IEEE Robot. Autom. Lett.*, vol. 7, no. 3, pp. 6155–6162, 2022.

[36] J. Lin, G. C. Thomas, N. V. Divekar, V. Peddinti, and R. Gregg, "A modular framework for task-invariant, energy shaping control of lower-limb exoskeletons," *TechRxiv*, 2023. [Online]. Available: https://doi.org/10.36227/techrxiv.24487378.v1

[37] K. Walters, G. C. Thomas, J. Lin, and R. D. Gregg, "An energetic approach to ankle exoskeleton control," in *2023 IEEE Int. Conf. Intell. Robots Syst.*, 2023, pp. 6082–6089.

[38] G. M. Bryan, P. W. Franks, S. C. Klein, R. J. Peuchen, and S. H. Collins, "A hip–knee–ankle exoskeleton emulator for studying gait assistance," *Int. J. Robot. Res.*, vol. 40, no. 4-5, pp. 722–746, 2021.

[39] U. H. Lee, C.-W. Pan, and E. J. Rouse, "Empirical characterization of a high-performance exterior-rotor type brushless dc motor and drive," in *2019 IEEE Int. Conf. Intell. Robots Syst.*, 2019, pp. 8018–8025.